77th IIW Annual Assembly and International Conference on Welding and Joining
7-12 July 2024
Rhodes, Greece

Effects of post-welded hot rolling on the properties of explosively welded Mg alloy/Al alloy cladding plates

Mami Mihara-Narita[1*], *Mingzhe* Bian[2], *Hisashi* Sato[1], *Yoshimi* Watanabe[1], and *Yasumasa* Chino[2]

[1]Department of Physical Science and Engineering, Nagoya Institute of Technology, 4668555 Nagoya, Japan
[2]National Institute of Advanced Industrial Science and Technology (AIST), 4638560 Nagoya, Japan

Abstract. The effects of hot rolling on the interfacial microstructure and mechanical properties of explosively welded Mg alloy/ Al alloy cladding plates with different thickness of Mg alloy were investigated. Explosively welded cladding plates showed wavy interface at the bonding interface. After hot rolling, the interface became flat and the voids at the interface disappeared. The presence of the interlayer was confirmed at the bonding interface in all samples. While the interlayer before rolling was single layer of a magnesium-rich γ-$Mg_{17}Al_{12}$ phase, after rolling it became double layer composed of γ-$Mg_{17}Al_{12}$ phase and aluminum-rich β-Al_3Mg_2 phase. Tensile strength increased as the initial thickness of the Mg alloy increased, and ductility was also improved. It was found that hot rolling was possible when both the roller temperature and sample temperature were set to 270 °C or higher, and when the only sample temperature was lowered to 250 °C. Tensile strength did not change significantly with temperature conditions, but elongation decreased with decreasing temperature conditions.

1 Introduction

In order to further reduce the weight of transportation equipment to improve fuel efficiency, lightweight and high-strength materials are required. In addition to aluminum (Al) alloys, which are used as lightweight materials for transportation equipment, the application of lightweight materials such as magnesium (Mg) alloys and carbon fiber reinforced plastics (CFRP) are also being widely considered. Mg alloys are expected to be a new lightweight material that can drastically reduce the weight of transportation equipment, but their low formability and corrosion resistance have become an issue [1-2]. Therefore, the development of clad materials, in which Mg alloys are combined with Al alloys, is attracting attention [3]. For example, if the clad materials are applied to transportation equipment, weight reduction can be expected. In addition, if Mg alloys are used for the hood and Al alloy for the frame, direct bonding of the two alloys is required. Here, the clad material can be expected to be used as a joint for both alloys.

For joining Mg alloys and Al alloys, interlayer composed of brittle intermetallic compound (IMC) phases [4-7], as shown in the phase diagram in Fig. 1 [8], form thickly at the bonding interface during fusion welding. The joint strength of the weld material is reduced by the formation of the interlayer. To solve this problem, explosive welding is applied to the dissimilar joining of these two alloys in this study. The explosive welding method is a type of solid-phase bonding that uses the energy released by the detonation of explosives to instantly bond dissimilar metal plates. Explosive welding is characterized by its high bonding speed and minimized formation of the interlayer at the bonding interface is hardly formed. In addition, since a wavy interface with a scale of several hundred micrometers is generally formed at the bonding interface, the anchor effect is expected to further increase the strength of the explosively welded material.

In practical application of explosively welded materials, it will be needed to control the thickness of welded material by hot plastic forming such as rolling. Although there are some reported cases [9-11] of secondary processing for the explosively welded Mg alloy/Al alloy cladding plates, there are many unknown points because the target of study is a specific alloy, and the investigation is insufficient for evaluation of required properties.

Our previous studies have confirmed the applicability of the explosive welding to the joining of Mg alloys to Al alloys [12, 13]. In addition, it was revealed that an annealing treatment after explosive welding increases the thickness of the interlayer formed at the bonding interface [14]. The interlayer was composed of a single layer of γ-$Mg_{17}Al_{12}$ phase after explosive welding. Thickness of the interlayer was less than 1 μm. However, after annealing at 200 °C for 24 hours, thickness of the interlayer increased to 2 to 4 μm and the interlayer exhibited a double-layer structure consisting of the γ-$Mg_{17}Al_{12}$ phase and β-Al_3Mg_2 phase.

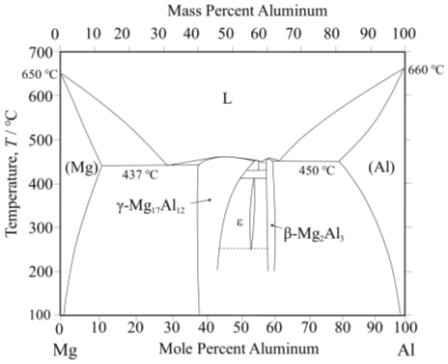

Fig. 1. Equilibrium phase diagram of Mg-Al system [5].

* Corresponding author: narita.mami@nitech.ac.jp

When the annealing temperature was further increased to 400 ℃ and kept for 1 hour, the thickness of the interlayer increased to 60 μm [15]. However, the effect of hot rolling on the microstructure and mechanical properties of the explosively welded material is not fully understood.

In this study, details of the interfacial microstructure of the bonding interface of explosively welded Mg alloy/Al alloy cladding plates with varying thicknesses of the Mg alloys by hot rolling are investigated. The purpose of this study is to clarify the effects of conditions during hot rolling on the joint interface microstructure and mechanical properties.

2 Experimental

The specimens used for explosive welding were extruded AZ31 Mg alloy and A6005C Al alloy. The alloy compositions are shown in Table 1. The thickness of the Al alloy was 3 mm, and the thickness of the Mg alloy was varied to 3 mm, 5 mm, and 8 mm. The total thicknesses of the explosively welded materials are 6 mm, 8 mm, and 11 mm, and are designated as explosively welded samples A, B, and C, respectively. For each of the samples, hot rolling was carried out up to a thickness of 3 mm with a rolling speed of 10 m/min. Sample temperature and roller temperature can be changed independently, and in this case both were set at 300 °C. A schematic diagram of the hot rolling process is shown in Fig. 2. The effects of the sample temperature and the roller temperature were also evaluated for the sample C. In this case, the sample temperature and the roller temperature were varied from 250 °C to 270 °C. The interfacial microstructure was observed by scanning transmission electron microscopy (STEM), and the mechanical properties of the samples were evaluated by tensile tests.

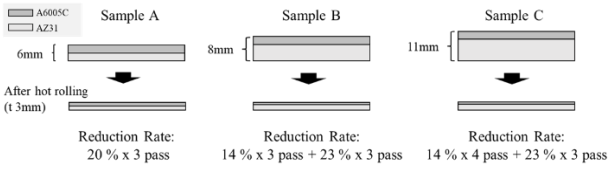

Fig. 2. Overview of hot rolling process. Sample temperature and roller temperature were set at 300 ℃. Additionally, for sample C, sample temperature and the roller temperature were varied from 250 ℃ to 270 ℃.

3 Results and Discussion

3.1 Characteristics of interfacial microstructure

Figure 3 shows the results of microstructure observation by optical microscopy at the bonding interface of sample A (a) before and (d) after rolling, sample B (b) before and (e) after rolling, and sample C (c) before and (f) after rolling. All samples showed a wavy interface unique to the explosively welded materials, and voids were observed near the interface in the samples B and C (allows are shown in Fig. 3 (b) and (c)). This is presumed to be due to a change in the impact force applied during detonation caused by increasing the thickness of the Mg alloy plate, resulting in voids at the bonding interface. After rolling, a flat interface was obtained in both cases, and the voids disappeared.

3.2 STEM observation for interfacial microstructure

Figure 4 shows STEM microstructures of the bonding interface before rolling in samples (a) A, (b) B and (c), (d) C. The presence of the interlayer at the bonding interface was observed in all samples (arrows in Fig. 4). Figure 5 shows STEM microstructures of the bonding interface after rolling in samples (a) A, (b) B and (c) C. While the interlayer before rolling was single layer, after rolling it became double layer. The interlayers on the Mg alloy side and the Al alloy side of the double layer structure are referred to as layer 1 and layer 2, respectively. From the results of line and point measurements by EDS, the interlayer of the single layer structure before rolling was estimated to be a magnesium-rich γ-$Mg_{17}Al_{12}$ phase. On the other hand, the double layer structure after hot rolling were estimated to be composed of magnesium-rich γ-$Mg_{17}Al_{12}$ phase and aluminum-rich β-Al_3Mg_2 phase for layer 1 and layer 2, respectively. As shown in Figs. 4(c) and 4(d), the thickness of the interlayer in sample C samples before rolling varied greatly depending on the observation areas.

Figure 6 shows the thickness of the interlayer in the samples after hot rolling. The thickness of the interlayer became the largest in sample C where the rolling cycles were more than in the case of samples A and B. Thickness of layer 2 (β-Al_3Mg_2 phase) was larger than that of the samples A and B. This may be caused by the longer time when the sample is exposed to high temperatures in sample C. In addition, the activation energy of the β-Al_3Mg_2 phase is lower than that of the γ-$Mg_{17}Al_{12}$ phase, and the β-Al_3Mg_2 phase tends to grow more easily [16], which may indicate the tendency for the β-Al_3Mg_2 phase with a larger thickness in the rolled samples. Similar tendency was confirmed in Mg/Al cladding samples fabricated by multi-pass hot roll bonding [17] and by twin-roll casting [18]. However, further investigation is required for clarification of formation and growth mechanism of the β-Al_3Mg_2 phase.

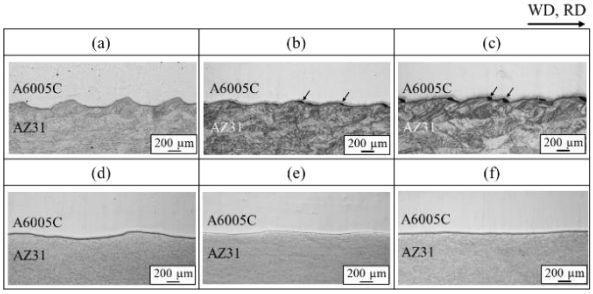

Fig. 3. Microstructures at the bonding interface of sample A (a) before and (d) after rolling, sample B (b) before and (e) after rolling, and sample C (c) before and (f) after rolling. Sample temperature and roller temperature were set at 300 ℃.

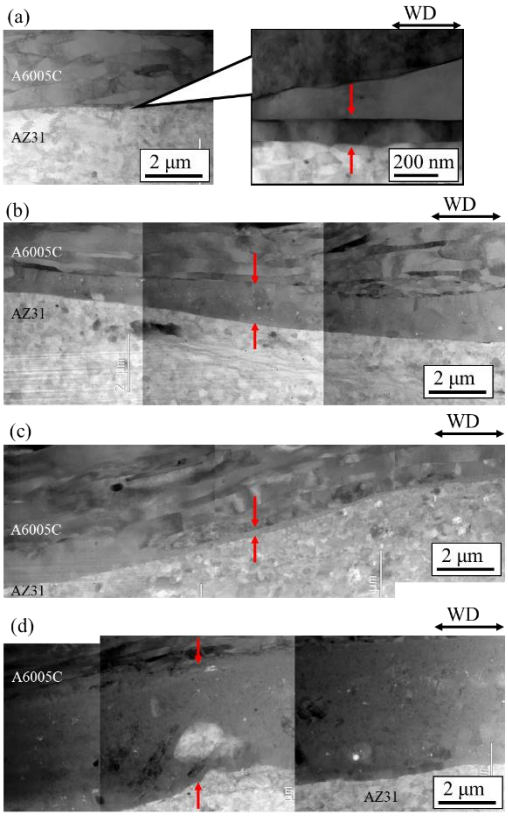

Fig. 4. STEM microstructures of the bonding interface before rolling in samples (a)A, (b)B and (c), (d)C.

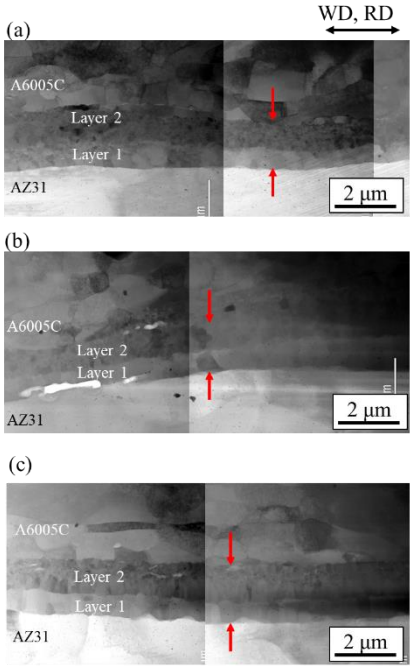

Fig. 5. STEM microstructures of the bonding interface after rolling in samples (a) A, (b) B and (c) C.

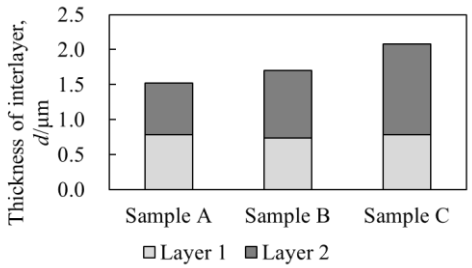

Fig. 6. Thickness of the interlayer in the samples after rolling. Sample temperature and roller temperature were set at 300 °C.

Figure 7 shows the results of EDS map analysis at the bonding interface of samples (a) A, (b) B and (c) C after rolling. In all samples, two transition regions were observed, which corresponded to the γ-$Mg_{17}Al_{12}$ phase and β-Al_3Mg_2 phase. Moreover, the distributions of Si atoms across the interface were readily observed in Fig. 7. It is assumed that because of the quicker diffusion rate of Al atoms, left behind impurity (Si) were observed in the β-Al_3Mg_2 layer near the Al alloy side. Similar phenomenon was observed in [19]. It is presumed that increased Si content at the interface may promote preferential formation of Mg_2Si and purify the base metal Al, which may improve the ductility of the bonded material. In addition to the thickness and constituent phases of the interlayer at the bonding interface, it is necessary to evaluate the relationship between the bonding strength and ductility by focusing on the Si distribution in the future.

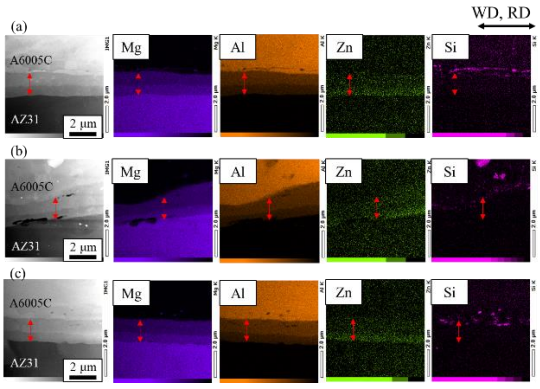

Fig. 7. Results of EDS map analysis at the bonding interface of samples in samples (a)A, (b)B and (c)C after rolling.

3.3 Formation of grain structure after rolling

Figure 8 shows inverse pole figure (IPF) maps overlapped on image quality (IQ) maps obtained by electron backscattered diffraction (EBSD) analysis at the bonding inteface in samples (a) A, (b) B and (c) C after rolling. In Mg alloy side, grains are recrystallized and formed small equiaxed grains. In Al alloy side, grains elongated in rolling direction are observed. Enlarged IPF maps with IQ maps obtained by EBSD analysis at the bonding inteface in samples (a) A, (b) B and (c) C after rolling are shown in Fig. 9. Interlayer locations (black coloured area) were not determined due

to low IQ values. Fine grains were observed on the Al alloy side near the bonding interface. On the Mg alloy side, the grain size tended to increase in the order of samples A, B, and C. The average grain size on the Mg-alloy side in the observed region in Fig. 9 was 7.1 μm, 6.1 μm, and 9.6 μm for samples A, B, and C, respectively.

Figure 10 shows pole figures for Mg alloy side of samples (a) A, (b) B and (c) C, and for Al alloy side of samples (d) A, (e) B and (f) C, respectively. Based on this, strong (0002) basal textures are confirmed in the Mg alloy side in all samples. On the other hand, rolling texure which appears in most hot-rolled Al alloys [20] is confirmed. No significant differences in texture were observed on either the Mg alloy or Al alloy side, depending on the sample.

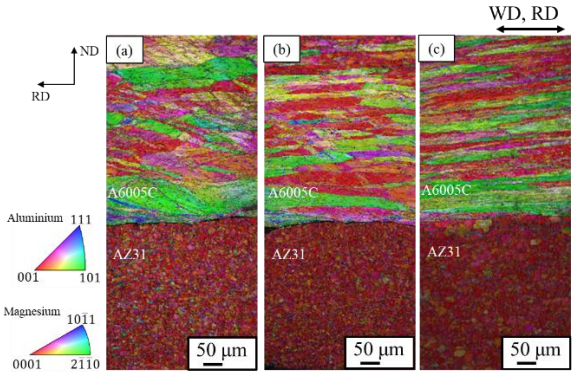

Fig. 8. IPF maps with IQ maps obtained by EBSD analysis at the bonding inteface in samples (a) A, (b) B and (c) C after rolling.

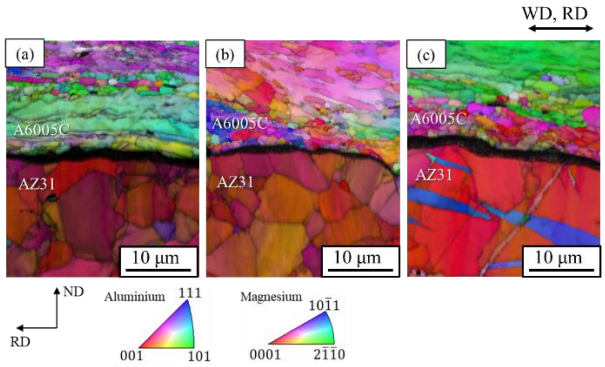

Fig. 9. Enlarged IPF maps with IQ maps obtained by EBSD analysis at the bonding inteface in samples (a)A, (b)B and (c)C after rolling.

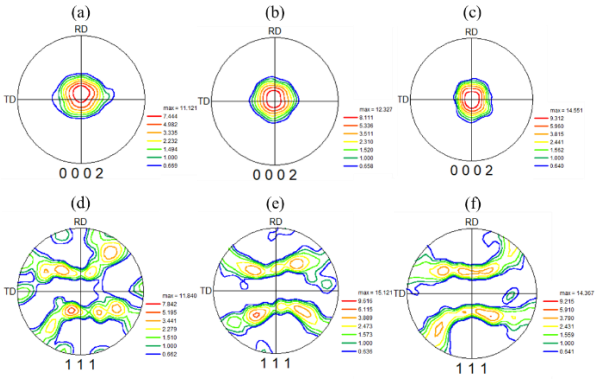

Fig. 10. Pole figures for Mg alloy side of samples (a) A, (b) B and (c) C, and for Al alloy side of samples (d) A, (e) B and (f) C, respectively.

3.4 Evaluation of mechanical properties by tensile tests

Figure 11 shows the results of tensile tests on the samples after rolling. The tensile test was performed perpendicular to the direction of explosive welding and rolling. The tensile strength increased as an increased in the initial thickness of the Mg alloy increased, and sample C had the highest strength and excellent ductility. From observations of the appearance of the samples after tensile test, fracture occurred due to cracking at the bonding interface in samples A and B. Although no figure is shown in the text, the fracture occurred at 45 degrees to the tensile direction in sample C. Figure 12 shows the results of fracture surface observation. In all samples, dimple structures, which are characteristic of ductile fracture, were observed on both Al alloy side and Mg alloy side. In the Mg alloy, a partially smooth fracture surface was also observed. A wavy shape was observed at the bonding interface. There was no significant difference in the morphology of the fracture surfaces among the samples.

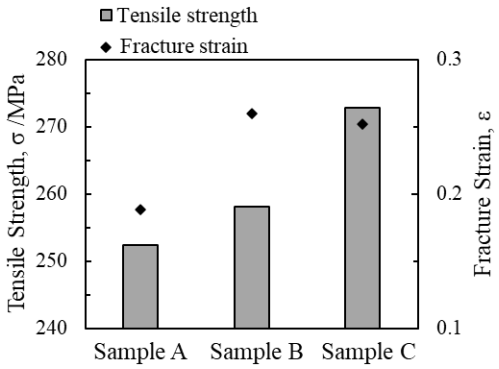

Fig. 11. Results of tensile tests after rolling.

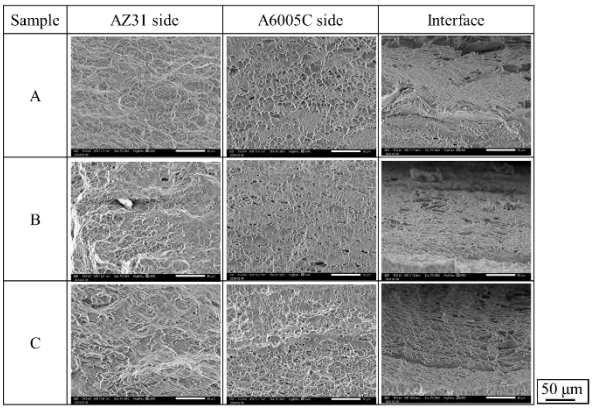

Fig. 12. Fracture surface after tensile test after rolling.

3.5 Effect of temperature conditions during rolling

The effects of sample temperature and roller temperature on sample C were investigated. When both the roller temperature and sample temperature were 250 °C, delamination occurred at the interface between the Mg alloy and Al alloy in the second pass of rolling. Rolling was possible when both the sample temperature

and roller temperature were set to 270 ℃ and when the sample temperature was lowered to 250 ℃. Figure 13 shows the microstructures of the bonding interface after rolling. In Fig. 13 (a), sample temperature and roller temperature were set as 270 ℃. On the other hand, in Fig. 13 (b), sample temperature was 250 ℃ and roller temperature was 270 ℃. In both cases, the bonding interface was flat, and no visible defects were observed.

Figure 14 shows the STEM microstructure of the bonding interface. When both the sample temperature and roller temperature were set to 270 ℃ (Fig. 14(a)), the microstructure was similar to that of the case where both temperatures were set to 300 ℃ (Fig. 5(c)), and the interlayer had a double layer structure. On the other hand, when the roller temperature was 270 ℃ and the sample temperature was 250 ℃ (Fig. 14(b)), the thickness of the interlayer became thinner.

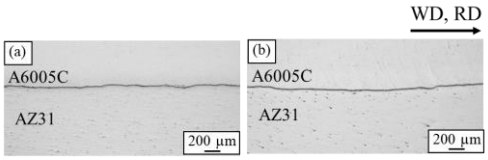

Fig. 13. Microstructures of the bonding interface of sample C after rolling. (a) Sample temperature: 270 ℃, roller temperature: 270 ℃, (b) sample temperature: 250 ℃, roller temperature: 270 ℃.

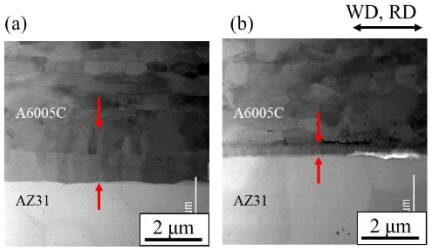

Fig. 14. STEM microstructures of the bonding interface of sample C after rolling. (a) Sample temperature: 270 ℃, roller temperature: 270 ℃, (b) sample temperature: 250 ℃, roller temperature: 270 ℃.

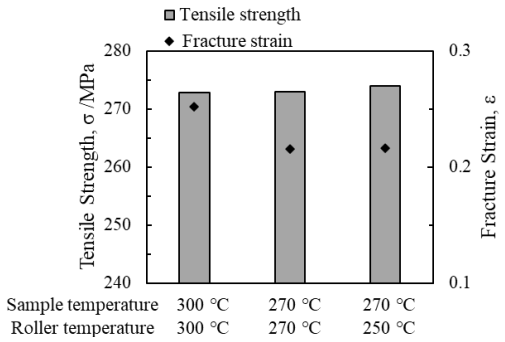

Fig. 15. Results of tensile tests after rolling for sample C.

Figure 15 shows the tensile strength and fracture strain obtained by test tests of sample C after rolling. There was no significant change in tensile strength depending on the temperature conditions during rolling. On the other hand, elongation decreased with decreasing temperature conditions during rolling. One potential factor is that the deformation capacity of the Mg alloy decreases at lower rolling temperatures. However, to elucidate the mechanism of changes in tensile properties, interfacial microstructure including crack initiation and propagation behavior should be clarified in the future.

4 Conclusions

In this study, hot rolling was applied to the explosively welded Mg alloy/ Al alloy cladding plates to analyze the interfacial microstructure in detail. In addition, the effects of temperature conditions during hot rolling on the interfacial microstructure and mechanical properties were investigated. Obtained results are summarized as follows.

(1) Explosively welded cladding plates showed wavy interface at the bonding interface. After hot rolling, a flat interface was obtained and the voids at the interface disappeared by hot rolling in all samples.

(2) In all samples, the presence of the interlayer was confirmed at the bonding interface. The interlayer was single layer before hot rolling and became double layer after hot rolling. The single layer was estimated to be a magnesium-rich γ-$Mg_{17}Al_{12}$ phase. On the other hand, the double layer after hot rolling was estimated to be composed of magnesium-rich γ-$Mg_{17}Al_{12}$ phase and aluminum-rich β-Al_3Mg_2 phase on the magnesium alloy side and aluminum alloy side, respectively.

(3) In the hot rolled samples, the tendency for the β-Al_3Mg_2 phase to have a larger thickness in the interlayer was obtained. This is because the activation energy of the β-Al_3Mg_2 phase is lower than that of the γ-$Mg_{17}Al_{12}$ phase, and the β-Al_3Mg_2 phase tends to grow more easily.

(4) Tensile strength increased as the initial thickness of the Mg alloy increased, and ductility was also excellent. There was no significant difference in the morphology of the fracture surfaces between the samples.

(5) As a result of changing the temperature conditions of hot rolling, it was confirmed that hot rolling was possible when both the sample temperature and roller temperature were set to 270 °C and when the only sample temperature was lowered to 250 °C. Tensile strength did not change significantly with temperature conditions, but elongation decreased with decreasing temperature conditions. Further investigation is needed on the interfacial microstructure including crack initiation and propagation behavior.

Acknowledgements: The authors would like to thank Asahi Kasei Corporation for providing the explosively welded cladding plates. This research was supported by the Light Metal Education Foundation, Japan and AMADA Foundation (AF-20021030-C2).

References

1. V.V. Joshi, S. Agnew, JOM, **69**, 2320 (2017)
2. T. Nakata, S. Kamado, J. Surf. Finish. Soc. Jpn., **71**, 200 (2019)
3. Y. Zhao, Z. Ding, Y. Chen, Mater. Charact., **128**, 156 (2017)
4. T. Morishige, A. Kawaguchi, M. Tsujikawa, M. Hino, T. Hirata, K. Higashi, Mater. Trans, **49**, 1129 (2008)
5. N. Yamamoto, J. Liao, S. Watanabe, K. Nakata, Mater. Trans, **50**, 2833 (2009)
6. Y. Zhao, Z. Lu, K. Yan, L. Huang, Mater. Des., **65**, 675 (2015)
7. M. R. Islam, M. Ishak, L. H. Shah, S. R. A. Idris, C. Meric, Int. J. Adv. Manuf. Technol., **88**, 2773 (2017)
8. T.B. Massalski, H. Okamoto, P.R. Subramanian, L. Kacprzak, Binary Alloy Phase Diagrams Second Edition (ASM International, 1990)
9. Z. Chen, D. Wang, X. Cao, W. Yang, W. Wang, Mater. Sci. Eng. A, **723**, 97 (2018)
10. M. Sahul, M. Sahul, J. Lokaj, L. Caplovic, P. Nesvadba, B. Odokienova, J. Mater. Eng. Perform., **28**, 6192 (2019)
11. M. Bian, X. Huang, N. Saito, Y. Chino, J. Alloy. Compd., **898**, 162957 (2022)
12. M. Mihara-Narita, K. Asai, H. Sato, Y. Watanabe, H. Mori, N. Saito, Y. Chino, J. Mater. Eng. Perform., **31**, 7039 (2022)
13. M. Mihara-Narita, H. Mori, H. Sato, Y. Watanabe, N. Saito, Y. Chino, H. Keno, Y. Yamada, T. Minoda, H. Tanaka, J. Light Met. Weld., **60**, 38 (2022)
14. M. Mihara-Narita, K. Asai, H. Mori, N. Saito, Y. Chino, H. Sato, Y. Watanabe, Weld. Int., **37**, 597 (2023)
15. H. Mori, M. Mihara-Narita, K. Asai, N. Saito, Y. Chino, T. Minoda, K. Kato, H. Tanaka, J. Light Met. Weld., **61**, 12 (2023)
16. S. Brennan, K. Bermudez, N.S. Kulkarni, Y. Sohn, Metall. Mater. Trans. A, **43A**, 4043 (2012)
17. P. Wang, Z. Chen, C. Hu, B. Li, T. Mo, Q. Liu, Mater. Sci. Eng. A, **792**, 139673 (2020)
18. J. Park, H. Song, J.-S. Kim, S.S. Sohn, S. Lee, Metall. Mater. Trans. A, **48**, 57 (2017)
19. J. Shang, K. Wang, Q. Zhou, D. Zhang, J. Huang, J. Ge, Trans. Nonferrous Met. Soc. China, **22**, 19611966 (2012)
20. J. Hirsch, T. Al-Samman, Acta Mater., **61**, 818 (2013)